Tensile Coupon Testing and Residual Stress Measurements of High-Strength Steel Built-Up I-Shaped Sections

KARA STALL, ANDREA CULHANE, LIKUN SUN, RACHEL CHICCHI CROSS, and MATTHEW STEINER

ABSTRACT

High strength structural steels (with yield stresses greater than 65 ksi) may have notably different material characteristics when compared to structural steels conventionally used in building construction [i.e., ASTM A992/A992M (2022) or A572/A572M Gr. 50 (2021)]. This paper presents findings from an experimental program that investigated the material characterization of ASTM A656/A656M Gr. 80 (2024) plate steel. The results obtained were compared to conventional ASTM A572/A572M Gr. 50 steel. Two types of testing were performed for this work: tensile coupon testing and residual stress testing. The tensile coupon testing was carried out for both the A656/A656M Gr. 80 and A572/A572M Gr. 50 plate material. The A656/A656M Gr. 80 plate material showed more variation between the two different plate thicknesses in both mechanical behavior and microstructure due to differences in steel production. The 0.375 in. thick plate exhibited a clear yield plateau with an ultimate/yield stress ratio similar to the Gr. 50 material. In contrast, the 0.5 in. plate did not have a yield plateau and reached lower ultimate strain. The residual stress testing was performed using a sectioning technique for one A572/A572M Gr. 50 and five A656/A656M Gr. 80 built-up sections that were fabricated from 0.5 in. and 0.375 in. plate material. Residual stresses obtained from measurements were compared to previously published predictive models. The ECCS model (ECCS, 1984) and BSK99 (Boverket, 2003) models were found to be reasonable predictors of residual stresses for all specimens except the one section fabricated from 0.5 in. thick Gr. 80 plate. When comparing the Gr. 50 and Gr. 80 specimens of the same cross-sectional geometry, the residual stresses were similar, implying that cross-sectional geometry is more prevalent than the nominal yield stress in determining residual stresses in built-up I-sections.

Keywords: high strength structural steel, mechanical properties, residual stress, built-up sections.

INTRODUCTION

High-strength structural steel (HS3) is being classified as any structural grade of steel with a yield stress, F_y, greater than or equal to 65 ksi (450 MPa). These higher strengths can be achieved through alloying, quenching and tempering, or thermo-mechanically controlled processing. Implementation of these high-strength steels has become increasingly popular in international markets, such as Europe and Asia; however, the United States has been slower to adopt their use. In 2019, the AISC Ad Hoc Task Group on High-Strength Steel published a final report (AISC, 2019) that discussed the benefits of HS3, paths forward for implementation into the AISC *Specification for Structural Steel Buildings* (AISC, 2022), hereafter referred to as the AISC *Specification*, and possible barriers that could block adoption of HS3 in the U.S. market.

Currently, select rolled shapes can be produced up to a yield stress of 80 ksi [ASTM A913/913M, Gr 80 (2019)] and plate material can be produced up to approximately 130 ksi. Although U.S.-based steel producers are capable of producing these HS3 products, a lack of guidance and standards has seemingly kept designers from implementing HS3 into their building designs, which has in turn limited the production of the material. This work is the beginning of a U.S.-based effort to study and promote the use of high-strength steel in buildings through better understanding of its behavior and realizing the potential of these materials.

One of the primary advantages of using HS3 in building applications is a potential reduction in steel tonnage when compared to the more conventional steel grades being used today. A higher yield strength may allow section sizes to be reduced and lead to material cost savings, faster

Kara Stall, PE, Graduate Research Assistant, Department of Civil and Architectural Engineering and Construction Management, University of Cincinnati, Cincinnati, Ohio. Email: pradzika@mail.uc.edu

Andrea Culhane, Graduate Research Assistant, Department of Civil and Architectural Engineering and Construction Management, University of Cincinnati, Cincinnati, Ohio. Email: clark3an@mail.uc.edu

Likun Sun, Graduate Research Assistant, Department of Mechanical and Materials Engineering, University of Cincinnati, Ohio. Email: sunlk@mail.uc.edu

Rachel Chicchi Cross, PhD, SE, Assistant Professor, Department of Civil and Architectural Engineering and Construction Management, University of Cincinnati, Cincinnati, Ohio. Email: rachel.cross@uc.edu (Corresponding)

Matthew Steiner, PhD, Assistant Professor, Department of Mechanical and Materials Engineering, University of Cincinnati, Ohio. Email: matt.steiner@ucmail.uc.edu

Paper No. 2023-14

erection times, reductions in foundation size, and reduced carbon emissions. ArcelorMittal has reported weight savings of 30% for columns that use Gr. 80 high-strength steel relative to conventional Gr. 50 steel. It also demonstrated potential fabrication cost savings of up to 46% when rolled high-strength steel shapes can be used in lieu of Gr. 50 built-up members that may be needed for very large loads (ArcelorMittal, 2019).

The mechanical properties of conventional (low carbon and/or high strength-low alloy) structural steel vary from HS3. A previous study completed by Ban et al. (2011) found that as the yield strength of the steel increased, the length of its yield plateau decreased until it completely disappeared in ultra-high-strength steels. This study also concluded that the value of ultimate strain decreased, and the yield/tensile ratio approached a value of 1.0 as the strength of the material increased. This can be seen in Figure 1, where an increase in material strength is generally accompanied by shorter strain-hardening regions, rupture at lower strain values, and a reduction in ductility. For some materials, an increase in material strength may also be accompanied by an elimination of the yield plateau within the stress-strain curve. However, the modulus of elasticity is unchanged; thus, to be utilized most effectively, HS3 should be used for force-controlled members instead of deflection-controlled members. It is important to note that while higher yield materials tend to see a reduction in ductility, this is due to specific processing choices and, if desired, higher yield materials can be produced with similar ductility properties to more conventional strength steels.

Residual stresses are formed in built-up sections due to uneven cooling during rolling of the individual plates and uneven heating during the welding process. Because residual stresses can greatly influence the behavior of a member, researchers have studied the stress distribution within steel sections, but work is needed to further evaluate built-up high-strength steel sections.

Several studies have been completed to investigate residual stresses in high-strength steel built-up members, and a summary of their results can be found in Table 1. Early research work by Rasmussen and Hancock (1995) found the average compressive stresses in the flanges and webs of S690 built-up sections to be $0.2F_y$ and $0.05F_y$, respectively. A study by Beg and Hladnik (1996) found that compressive residual stresses in the flanges of 700 MPa (100 ksi) built-up members ranged from $0.09–0.14F_y$. Studies by Ban et al. (2013) and Wang et al. (2012) conducted on 460 MPa (65 ksi) built-up I-sections found that average compressive residual stresses in the flanges increased as the sections became more compact. Testing completed by Liu (2017) found that residual stresses in S690 (100 ksi) built-up sections were "proportionally less" when compared to the residual stresses in S355 (50 ksi) members. This finding was also observed by Schaper et al. (2022), who studied residual stresses in cross sections fabricated from S355 (50 ksi) and S690 (100 ksi) steel material. They found that the cross-sectional geometry has a much larger influence on the residual stresses than the material strength. Specifically, they found that narrower flanges led to higher compressive residual stresses, and thinner flanges caused larger tensile stresses at the mid-point of the flanges.

Another study was completed by Simoes da Silva et al. (2021), and results were published in a report by STROnger steels in the Built Environment (STROBE.) This study measured residual stresses in the flanges and webs of built-up I-shaped sections consisting of S690 (100 ksi) and S460 (65 ksi) steel material. Results from this study found that maximum tensile stresses in the flanges were comparable to European Convention for Constructional Steelwork (ECCS, 1984) recommended values, but the measured

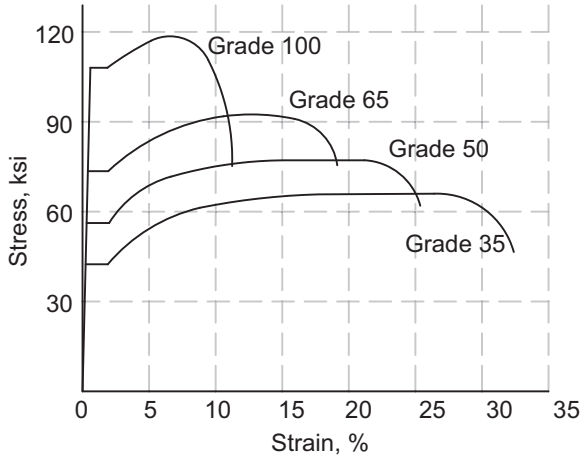

Fig. 1. Comparison of stress-strain relationships for different steel grades (NSC, 2015).

Table 1. Residual Stress Values from Literature							
			Specimen Thickness (nominal)		Average Compression Stress		Peak Tension Stress
Reference	Specimen	Steel Strength MPa	Web mm	Flange mm	Web MPa	Flange MPa	Flange MPa
Rasmussen and Hancock (1995)	N/A	690	8	8	32	135	NR
Beg and Hladnik (1996)	B	700	10	12	NR	73	NR
	D		10	12		123	
Ban et al. (2013)	RI1-460	460	10	10	233.9	276.6	277.5
	RI2-460		10	10	208.4	206.5	317.1
	RI3-460		14	14	123.7	93.0	254.9
	RI4-460		10	10	213.8	163.8	337.0
	R15-460		12	12	65.2	50.9	153.6
	RI6-460		10	12	74.9	80.4	135.8
	RI7-460		10	12	91.4	78.0	189.9
	RI8-460		10	10	142.2	190.6	301.2
Wang et al. (2012)	R-H-3	460	11	21	69.9	187.7	477.9
	R-H-5		11	21	108.1	124.7	414.0
	R-H-7		11	21	60.3	89.7	336.3
Liu (2017)	C1R-A	690	6	10	98.1	206.1	357
	C2R-A		6	10	75.9	214.1	452
	C3R-A		10	16	138.0	138.0	368
	C4R-A		10	16	133.4	120.3	354
Wang (2018)	B2	690	6	10	116	157	400
	B4		6	16	68	67	111
	B6		6	10	126	138	453
Schaper et al. (2022)	1fy	460	8	20	45.9	59.8	329
	3-1fy	460	8	20	46.1	104.2	329
Simoes de Silva (2021)	C1	690	8	8	170	42	336
	C2	690	8	8	235	156	336
	C3	690	8	16	150	116	484
	C4	690	8	16	112	85	237
	B1	460	8	16	101	75	228
	B2	690	8	16	80	63	277
	B3	460	10	16	20	83	118
	B4	460	8	16	107	57	310
	B5	690	8	16	69	53	357
	B6	460	9	15.5	160	32	113
	B7	690	8	16	72	83	339
	BC-1	690	8	16	87	72	145

NR = Not reported

Table 2. Tensile Coupon Test Matrix	
Plate Material and Thickness	**Number of Tests**
A572-50_0.375 in.	12 (6L and 6T)
A572-50_0.5 in.	12 (6L and 6T)
A656-80_0.375 in.	12 (6L and 6T)
A656-80_0.5 in.	12 (6L and 6T)
L = Longitudinal direction, T = Transverse direction	

average compressive stresses were higher than the ECCS values. The higher compressive stresses were attributed to the measured tensile residual stresses at the flange tips due to the plates being flame cut during the fabrication process.

This paper focuses on the stress-strain behavior and residual stresses of built-up I-shape sections using ASTM A656/A656M Gr. 80 (2024) material, hereafter referred to as A656-80, relative to conventional ASTM A572/A572M Gr. 50 (2021) material, hereafter referred to as A572-50. A656 steel is commonly used for applications such as construction equipment, crane booms, heavy vehicle frames, and rail cars; while it may be useful in building applications, it is not currently included as a listed material in the AISC *Specification* (AISC, 2022). A656-80 material was used due to material availability at the time of the study and even though it is not typically used for building applications, it does have a comparable yield/tensile ratio and elongation value when compared to A913/A913M Gr. 80 steel, hereafter referred to as A913-80. Both A656 and A913 materials are high-strength low-alloy products, but A913 is specifically produced by quenching and self-tempering. A656 also has a thickness limit of 1 in. for its Gr. 80 material.

TENSILE COUPON TESTING

A total of 48 coupon tests were performed in this experimental program. The test matrix is shown in Table 2, which shows a combination of A572-50 and A656-80 plate in thicknesses of 0.375 in. and 0.5 in. The coupon specimens and testing protocols conformed to the ASTM A370-20 specification (ASTM, 2020) for subsize specimens. Each of the coupons were cut with a waterjet cutting machine in both the longitudinal and transverse directions relative to the rolled direction of the plate. The coupons were unfortunately returned unmarked, so the differentiation of rolling direction could not be determined. However, the data collected was very similar, so it is presumed that there was little to no difference between the longitudinal and transverse coupons.

A hydraulic-controlled Material Testing Systems (MTS) machine with wedge grips and an axial load capacity of 22 kips was used to perform the tensile coupon tests. An extensometer with a gage length of 1 in. was attached to the coupon specimens during testing to collect strain data. To avoid any possible damage to the extensometer at rupture, the testing program was set to be force controlled during the elastic region and then shifted to displacement controlled during the inelastic region. The testing program for the A656-80 coupons started as force controlled at 1 kip/min up to a maximum of 5 kips, and then switched to displacement controlled at a rate of 0.1 in/min to a maximum of 0.5 in. The testing program for the A572-50 coupons used the same force and displacement loading rates as the A656-80 tests with maximums of 3.5 kips and 0.65 in., respectively. Figure 2 shows the tensile coupon test setup with the extensometer attached at the center of the tensile specimen.

Tensile Coupon Testing Results

Table 3 reports the average modulus of elasticity, E, yield stress, F_y, yield strain, ε_y, tensile stress, F_u, tensile strain, ε_u, and strain at fracture, ε_f, measured for each of the plate material types and thicknesses. The 2% offset method was used to calculate the yield stress of each coupon. The standard deviation among the 12 tests for each category is provided in parentheses. As expected, the modulus of elasticity was comparable among the four-test series. The ratio F_y/F_u provides an indication of the material overstrength; the 80 ksi material exhibited ratios closer to 1.0. The strain hardening region, as demonstrated by the ratio $\varepsilon_u/\varepsilon_y$, was shorter for the 80 ksi material. The Gr. 80 material also exhibits lower ductility overall, as evidenced by the ratio $\varepsilon_f/\varepsilon_y$.

Figure 3 shows full stress-strain curves for each series of the material types and thicknesses that were tested. The graph presents the stress-strain curves for each of the 12 tests per material and thickness type. In order to avoid damaging the extensometer during testing, it was removed from

Table 3. Measured Material Properties from Tensile Coupon Tests[a]									
Plate Material	***E*** **ksi**	F_y **ksi**	F_u **ksi**	ε_y **%**	ε_u **%**	ε_f **%**	F_y/F_u	$\varepsilon_u/\varepsilon_y$	$\varepsilon_f/\varepsilon_y$
50 ksi 0.375 in.	28695 (460)	63.2 (1.00)	72.6 (0.84)	0.42 (6.8E-3)	15.5 (1.09)	28.4 (1.17)	0.87	36.9	67.6
50 ksi 0.5 in.	28282 (579)	58.1 (0.73)	71.8 (0.60)	0.41 (6.8E-3)	17.8 (0.57)	30.6 (0.89)	0.81	43.4	74.6
80 ksi 0.375 in.	29058 (959)	98.9 (0.89)	110.4 (0.51)	0.55 (7.8E-3)	12.2 (0.33)	22.9 (0.58)	0.90	22.2	41.6
80 ksi 0.5 in.	27846 (443)	83.9 (0.59)	92.1 (1.33)	0.50 (6.7E-3)	8.36 (0.35)	19.4 (1.03)	0.91	16.7	38.8

[a] Standard deviation among coupon test results is listed in parentheses

Fig. 2. Tensile coupon test setup.

the specimen at approximately 10–15% elongation of the coupon. Strains beyond approximately 10–15% were calculated based on the recorded displacement of the test frame.

It can be seen from Figure 3 that there was not a significant deviation in recorded stress among each test within the series. The strain at rupture was more variable within each test series. The A572-50 plate material produced very similar behavior for both the 0.5 in. and 0.375 in. plate material, while the A656-80 curves have a much more significant variation between the two thicknesses. The A656-80 0.5 in. plate exhibited almost no yield plateau, and its yield stress was much lower than the 0.375 in. plate. In contrast, despite its high strength, the A656-80 plate with 0.375 in. thickness behaved like more conventional steels with an established yield plateau and with comparable ductility and ultimate/yield stress ratios.

The differences between the Gr. 80 stress-strain curves for the 0.375 in. and 0.5 in. materials can be attributed largely to microstructural differences between the two plates, as these materials were produced by different steel producers. Table 4 shows the mill-certified chemical compositions for each of the plate materials that were tested. Comparing the A656-80 0.5 in. plate to the A656-80 0.375 in. plate, there are differences, but no major outliers, in the minor alloying elements added to provide higher strength and greater toughness. The microstructures of the two Gr. 80 plates, however, are significantly different from each other and explain the variation in mechanical behavior.

Analyses of Steel Microstructures

Samples from each plate along each of the three primary directions (rolling, transverse, plate normal) were sectioned and prepared to a mirror finish using standard metallographic techniques, then etched (2% nitric acid in methanol) to reveal both the ferritic grain boundaries and carbides under optical microscopy. The 0.375 in. Gr. 80 plate exhibits a nearly homogenous microstructure of both equiaxed

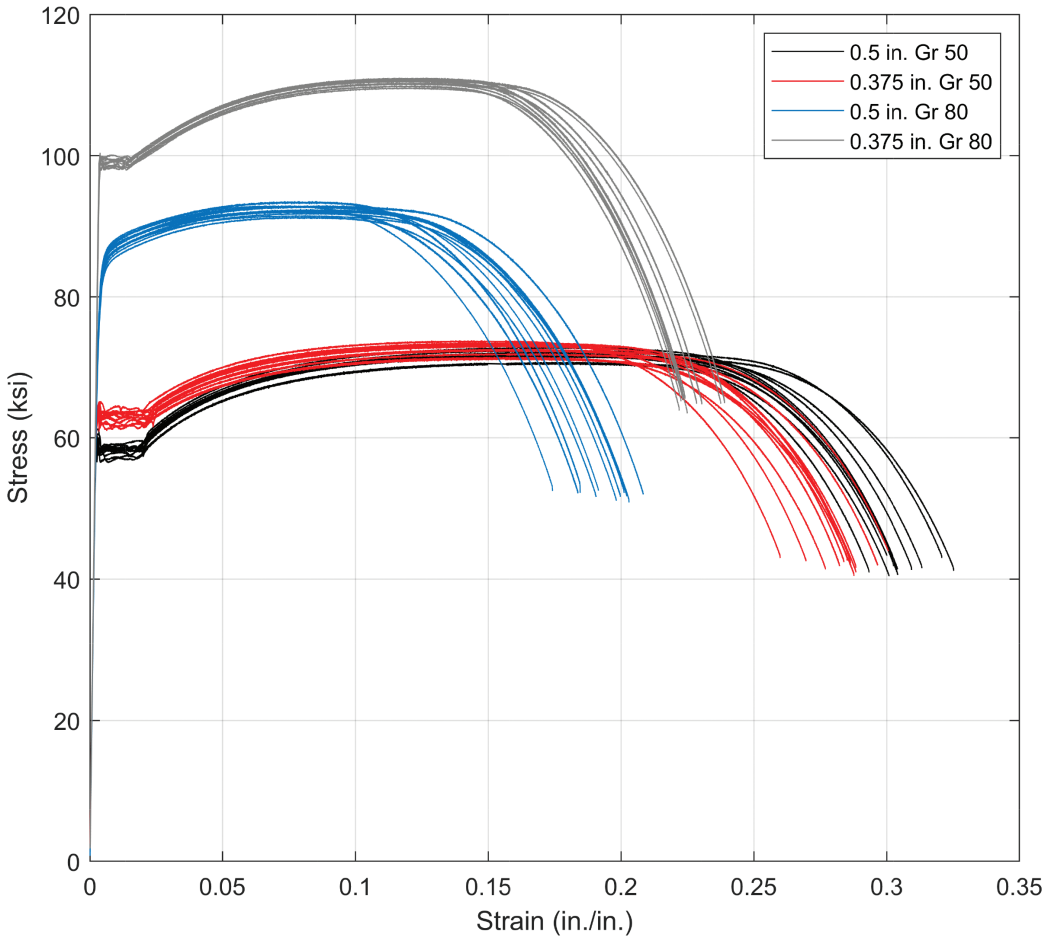

Fig. 3. Measured engineering stress-strain curves for each plate type.

Table 4. Plate Chemical Compositions					
	A572-50 0.375 in. PL %	A572-50 0.5 in. PL (1)[a] %	A572-50 0.5 in. PL (2)[a] %	A656-80 0.375 in. PL %	A656-80 0.5 in. PL %
C	0.04	0.06	0.06	0.06	0.07
Mn	0.8	0.82	0.83	1.45	1.48
P	0.01	0.012	0.014	0.014	0.013
S	0.002	0.007	0.006	0.004	0.003
Si	0.05	0.02	0.02	0.02	0.1
Al	0.023	0.038	0.039	0.028	0.043
Cu	0.08	0.13	0.13	0.1	0.02
Ni	0.03	0.05	0.05	0.05	0.01
Cr	0.08	0.07	0.09	0.06	0.04
Mo	0.02	0.02	0.02	0.09	—
Sn	0.005	0.03	0.03	0.006	0.001
Ti	0.001	0.002	0.002	0.106	0.07
V	0.002	0.002	0.003	0.007	0.003
Nb	0.047	0.024	0.026	0.034	0.032
N	0.008	0.007	0.008	0.0109	0.0048
B	0.0003	0.0001	0.0001	0.0007	0.0002
Ca	0.002	0.0026	0.0023	0.0007	0.0014
Zr	0.0003	—	—	—	—
Sb	—	0.001	0.001	—	0.001

[a] A572-50 0.5 in. plate material came from two different heats and, thus, the two different chemistries shown in the table for this plate type. All other plate types were from a single heat.

and acicular ferrite with a fine grain size and a uniform distribution of carbides (Figure 4). In contrast the 0.5 in. Gr. 80 plate presents a more conventional rolled microstructure with larger ferrite grains found in bands and elongated along the rolling direction (RD), interspersed with lamellar pearlite colonies (dark regions) in addition to the smaller carbides. Based upon these microstructures, it is clear that the two plates, sourced from different suppliers, were likely produced via different methods. The refined polygonal ferrite grains, acicular ferrite, and fine dispersed precipitates of the 0.375 in. Gr. 80 plate are consistent with what would be expected to be produced via a thermo-mechanically controlled process (TMCP) or similar processing route (Sampath, 2005). The 0.5 in. Gr. 80 plate with the banded structure of elongated grains and pearlitic colonies appears to have been controlled rolled and differs from the 0.5 in. Gr. 50 plate primarily in having a smaller grain size and a narrower grain size distribution (Figure 5). Consistent with the mechanical behavior in Figure 3, the microstructure of the 0.375 in. Gr. 80 would be expected to exhibit both a higher yield strength and improved toughness compared to the microstructure of the 0.5 in. Gr. 80 plate.

Results from the microstructure analysis leads to the important conclusion that just knowing the yield strength of the material and its chemical composition may not be enough to accurately predict the material behavior. It will become increasingly important to understand how different rolling processes will affect the microstructure of the steel and ultimately material behavior, especially if different processes will result in such a large difference in material properties.

RESIDUAL STRESS TESTING

Experimental Test Specimens

Six built-up I-shaped specimens were fabricated from 0.375 in. and 0.5 in. thick Gr. 50 and Gr. 80 plate material in order to measure residual stresses. The plates were cut to size using waterjet cutting and then fillet-welded using automated welding collaborative robots. Five different

cross sections were fabricated using Gr. 80 steel and one section was fabricated with Gr. 50 steel in order to provide a comparison between the two materials. These sections and others are to be subjected to stub column testing in the future. The cross sections used in this study were admittedly small due to plate availability and limitations with the testing equipment available to apply adequate compressive load during column testing. Yet, they provide a valuable comparison between the conventional Gr. 50 material and the higher strength material.

Table 5 and Figure 6 display the section properties and dimensions of each built-up section using the naming convention "I nominal yield strength–b/t ratio–h/t ratio." The ratios, b/t and h/t, reflect the slenderness of the flange and web elements, respectively, by calculating the width, b or h, divided by the thickness, t. The cross-sectional slenderness

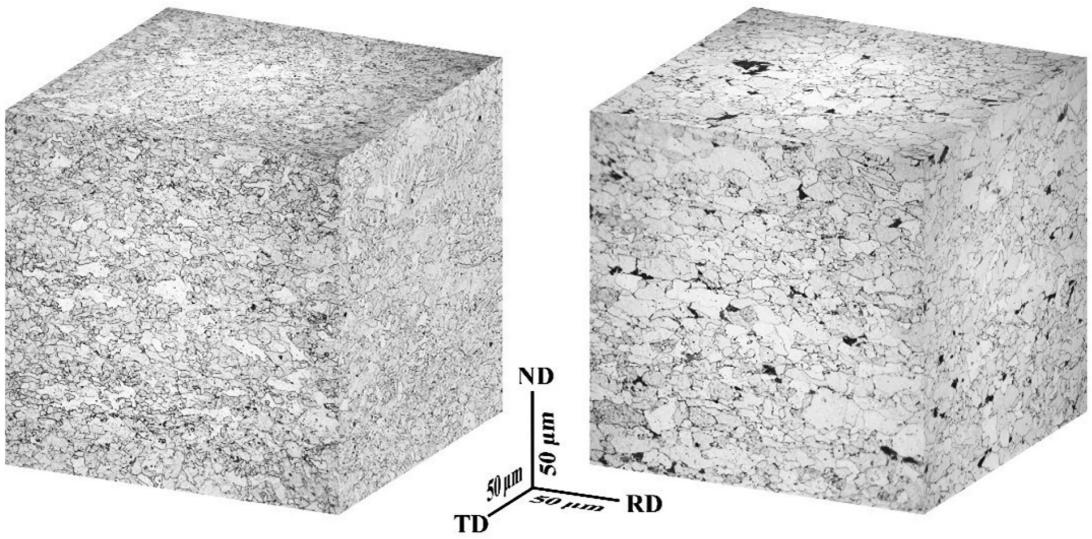

(a) 0.375 in. *(b) 0.5 in.*

Fig. 4. Psuedo-3D microstructural reconstructions of the. Gr. 80 plates (RD = rolling direction, TD = transverse direction, ND = normal direction).

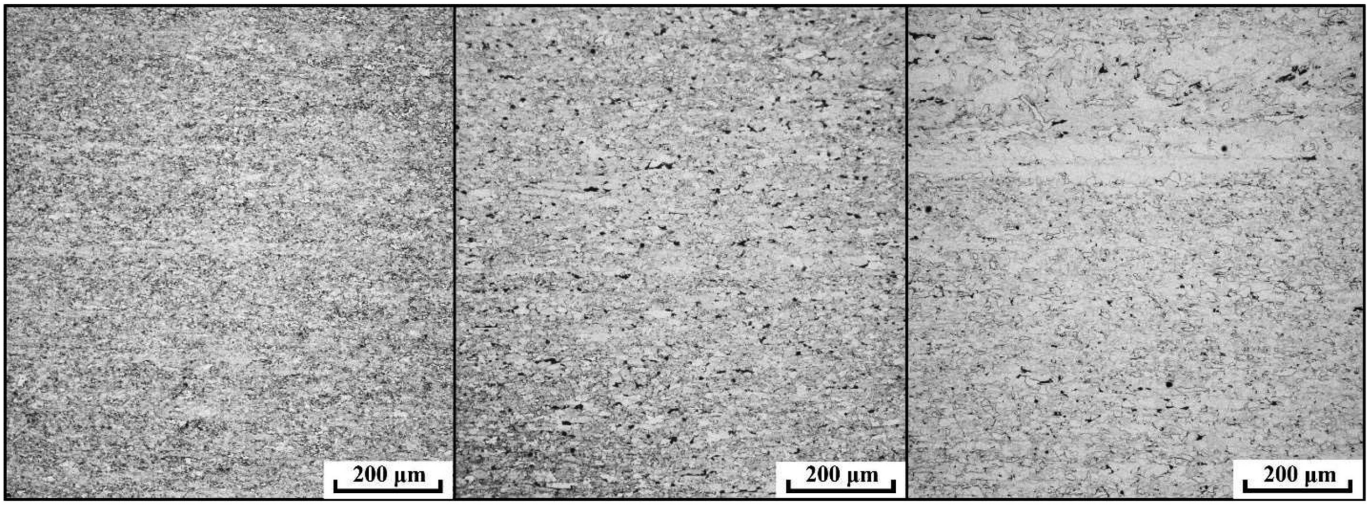

(a) 0.375 in. Gr. 80 *(b) 0.5 in. Gr. 80* *(c) 0.375 in. Gr. 50*

Fig 5. Microstructural cross sections of the plates (RD = rolling direction, TD = transverse direction, ND = normal direction).

Table 5. Specimen Section Properties									
Specimen Name[a]	F_y ksi	Length in.	b in.	h in.	t in.	b/t	h/t	λ_{rf}[b]	λ_{rw}[c]
I 80-5.3-32	80	48	2	12	0.375	5.3	32.0	10.2	28.4
I 80-9.3-28	80	43.5	3.5	10.5	0.375	9.3	28.0	10.6	28.4
I 80-10.7-21.3	80	36	4	8	0.375	10.7	21.3	10.6	28.4
I 80-10.7-32	80	48	4	12	0.375	10.7	32.0	10.2	28.4
I 80-4-24	80	48	2	12	0.5	4.0	24.0	10.6	28.4
I 50-10.7-32	50	48	4	12	0.375	10.7	32.0	13.0	35.9

[a] Specimen naming convention: I "steel grade" – "b/t ratio" – "h/t ratio"
[b] λ_{rf} limiting ratios were calculated from AISC *Specification* Table B4.1a for Case 2 (flanges of I-shaped built-up sections).
[c] λ_{rw} limiting ratios were calculated from AISC *Specification* Table B4.1a for Case 5 (webs of I-shaped built-up sections).

limiting ratios, λ_{rf} and λ_{rw}, shown in Table 5 were calculated from AISC *Specification* Table B4.1a. It is important to note that the applicability of these equations have not yet been evaluated for Gr. 80 steel but will be explored in the future stub column testing of these specimens. Efforts were made to select cross-sections of various slenderness ratios relative to the slenderness limiting ratios. The Gr. 50 specimen had the same cross section as one of the Gr. 80 specimens.

Residual Stress Measurement Procedure

Residual stress testing was performed on six specimens and was completed using the sectioning technique outlined in Technical Memorandum No. 6 of the Structural Stability Research Council (SSRC) *Guide to Stability Design* (Ziemian, 2010). This common sectioning approach assumes for simplicity that transverse stresses in the specimen are negligible. The residual stress specimens were fabricated to the lengths shown in Table 5, which conform to the SSRC *Guide*. A 12 in. test piece was then marked at the center of each specimen as shown in Figure 7. The test piece was then marked into 0.5-in.-wide strips along the top and bottom flanges and the web. Using a mill, holes were drilled into each test strip, 1 in. from each end, which provided a gauge length of 10 in.

Initial measurements between the holes were taken using a gauge similar to a Wittemore strain gauge, shown in Figure 8. This gauge has a tolerance of 0.0001 in. and a nominal gauge length of 10 in. When taking measurements, the gauge is used to measure the reference bar before and after each set of measurements. If the reference bar measurements vary by more than 0.001 in, then the temperature has changed, and the measurement set would need to be repeated.

After the collection of all initial measurements, the specimens were cut down using a waterjet. The waterjet was

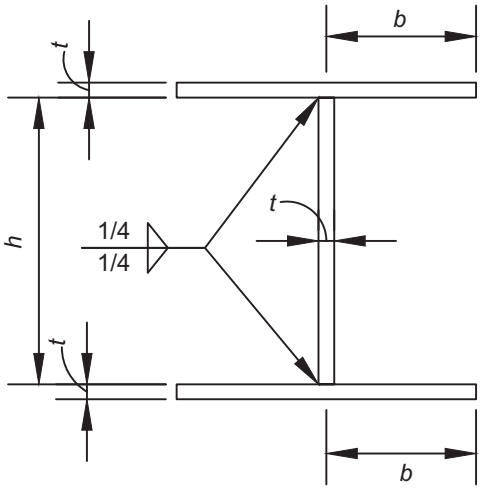

Fig. 6. Geometric dimensions.

used to minimize the amount of heat and stress that would be added to the specimen. The test piece was first cut from the full-length specimen, and then the test piece was cut down into its three main components (top flange, bottom flange, and web). Each component was then cut into its marked 0.5 in. strips. Figure 9 shows a fully sectioned test piece. Once the test piece had been fully sectioned into the 0.5 in. strips, all pieces were dried off and left overnight to come to room temperature. The final gauge length measurements were taken and followed the same procedure that was used for the initial measurements. The change in deformation recorded from the measurements was then converted into stresses using Hooke's law.

Due to limitations with the waterjet nozzle, the test strips at the flange-web interface were L-shaped, as shown in Figure 10, with an approximate thickness of 1 in. The final gauge length measurements were first taken when the strips were in this configuration. The excess material (weld and web) was then removed using a vertical band saw and mill, and measurements were taken again. Both sets of results are presented.

Residual Stress Results

The residual stress results that are presented in this section have been compared with previously published predictive models. The comparison models chosen for this work are

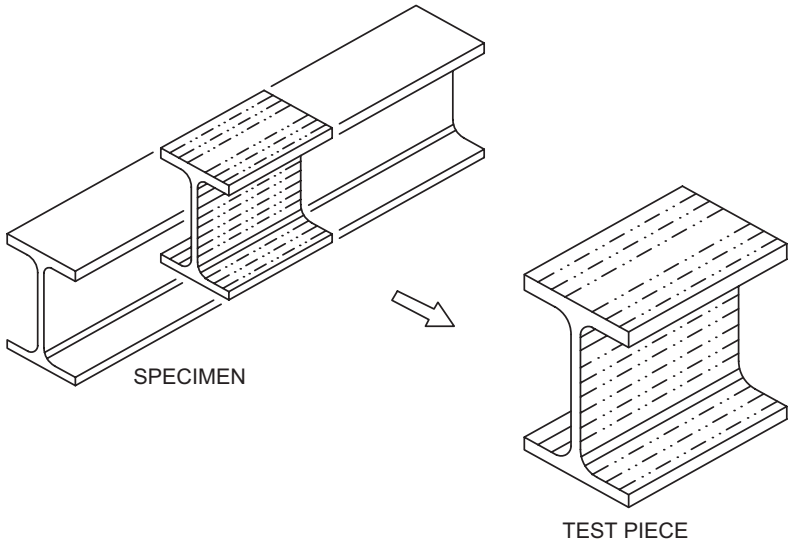

Fig. 7. Residual stress sectioning method schematic (Ziemian, 2010).

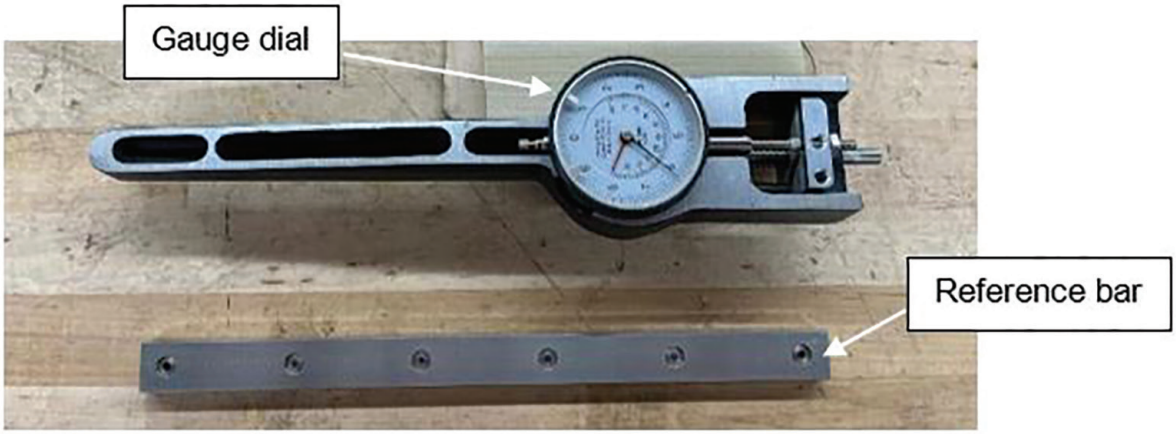

Fig. 8 Gauge to measure strain.

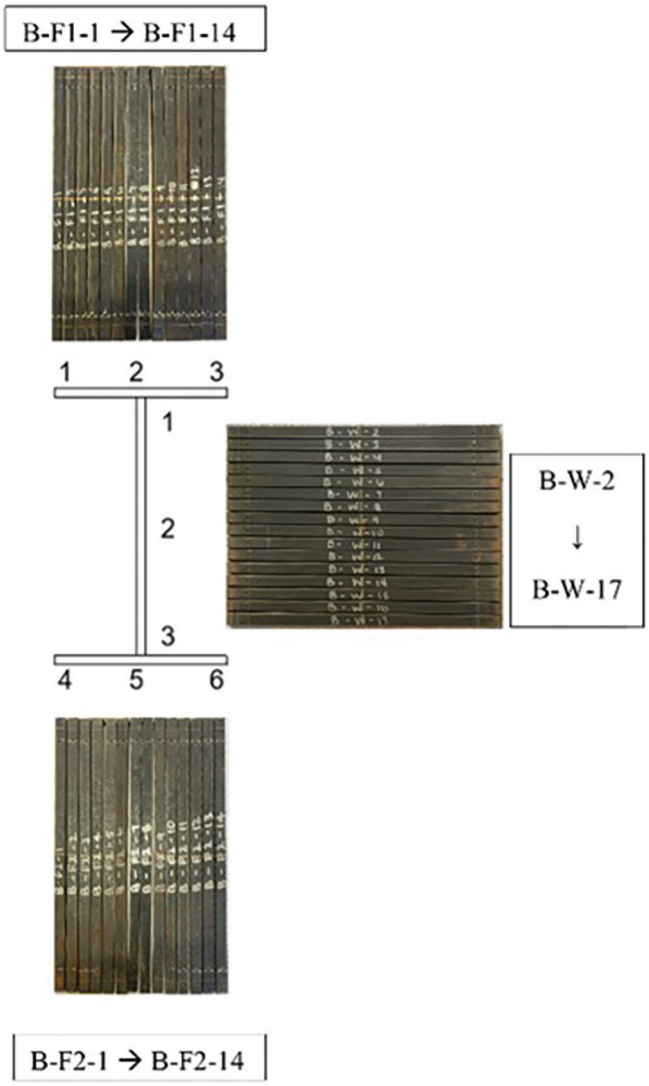

Fig. 9. Fully sectioned specimen I 80 9.3-28R.

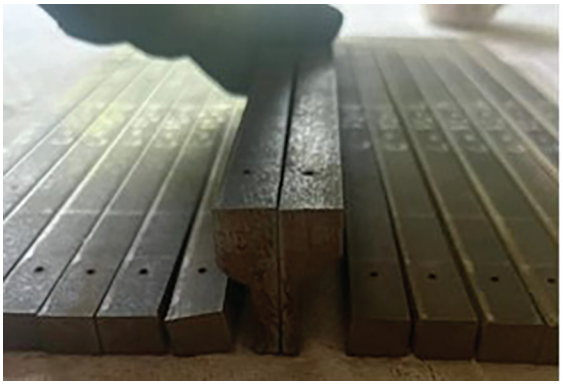

Fig. 10. L-shaped sections at flange-web interface.

Table 6. Residual Stress Predictive Models for Welded I-Sections						
Predictive Model	**Peak Tensile Residual Stresses**	**Peak Compressive Residual Stresses**	***a***	***b***	***c***	***d***
ECCS (ECCS, 1984)	$1.0F_y$	$0.25F_y$	$0.05b_f$	$0.15b_f$	$0.075h$	$0.05h$
BSK 99 (Boverket, 2003)	$1.0F_y$	From equilibrium	$0.75t_f$	$1.5t_f$	$1.5t_w$	$1.5t_w$
Y. SUN (Sun, 2019)	$0.8F_y$	From equilibrium	$0.225b_f$	$0.15b_f$	$0.075h$	$0.225h$
Note: b_f = flange width, h = clear distance between flanges, t_w = web thickness, t_f = flange thickness						

Table 7. Peak and Average Residual Stress Values vs. Predictive Models									
	Web Compression Stress (ksi)			**Flange Compression Stress (ksi)**			**Flange Tensile Stress (ksi)**		
		Predicted Value			**Predicted Value**			**Predicted Value**	
Specimen	**Measured**	**ECCS**	**BSK 99**	**Measured**	**ECCS**	**BSK 99**	**Measured**	**ECCS**	**BSK 99**
I 80-5.3-32	21.2	20	21.8	11.9	20	21.7	61.9	80	80
I 80-9.3-28	16.6	20	11.9	11.1	20	11.3	51.9	80	80
I 80-10.7-21.3	9.2	20	9.5	18.3	20	9.5	74.7	80	80
I 80-10.7-32	8.9	20	9.9	19.4	20	9.5	71.2	80	80
I 80-4-24	12.3	20	31.0	9.6	20	31.2	14.5	80	80
I 50-10.7-32	13.0	12.5	6.0	11.9	12.5	6.2	54.2	50	50

predictive models by the ECCS (1984); the Swedish regulations BSK 99 (Boverket, 2003); and a proposed numerical model completed by Sun et al. (2019), called the Y.SUN model in this study. A summary of these three models can be found in Table 6. Each of these predictive models follow a residual stress distribution pattern that is presented in Figure 11.

Measured residual stress values for each of the six specimens are shown in Figure 12. Values in gray are the measured residual stress values prior to the excess web material being removed from the flange test strips. The values in black are the measured values after removal. Table 7 presents key residual stress values for each specimen with a comparison to the corresponding values from the predictive models in Table 6. The tensile stress in the flanges is provided as a peak value, while the compressive stress values are taken as an average of all values recorded over the width of the flange or web.

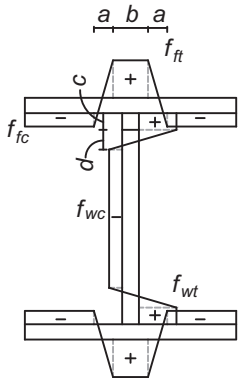

Fig. 11. General residual stress pattern for welded I-shaped sections (ECCS, 1984).

Figure 13 presents the predictive model comparison results for specimen I80-10.7-21.3R. Overall, the compressive stresses in the flanges were most accurately predicted by the ECCS (1984) model, while the peak tensile stress in the flange was closest to the Y.SUN (Sun, 2019) model for the top flange, *F1*, and the ECCS and BSK 99 (Boverket, 2003) models for the bottom flange, *F2*. The transition zone slopes fall somewhere between the ECCS and BSK 99 models.

Figure 13(c) presents the results for the compressive residual stresses in the web of specimen I80-10.7-21.3. The stresses measured were fairly uniform along the full depth of the web, at a measured value of approximately 10 ksi (12.5% of nominal F_y). These stresses are most accurately predicted by the BSK 99 (Boverket, 2003) model. Due to the size of the strain gauge, measurements were unable to be taken close enough to the flange-web interface to measure results in the tensile stress region of the web, so no comparison can be made to the predictive models in that region. The results for specimens I80-10.7-32R and I50-10.7-32R closely

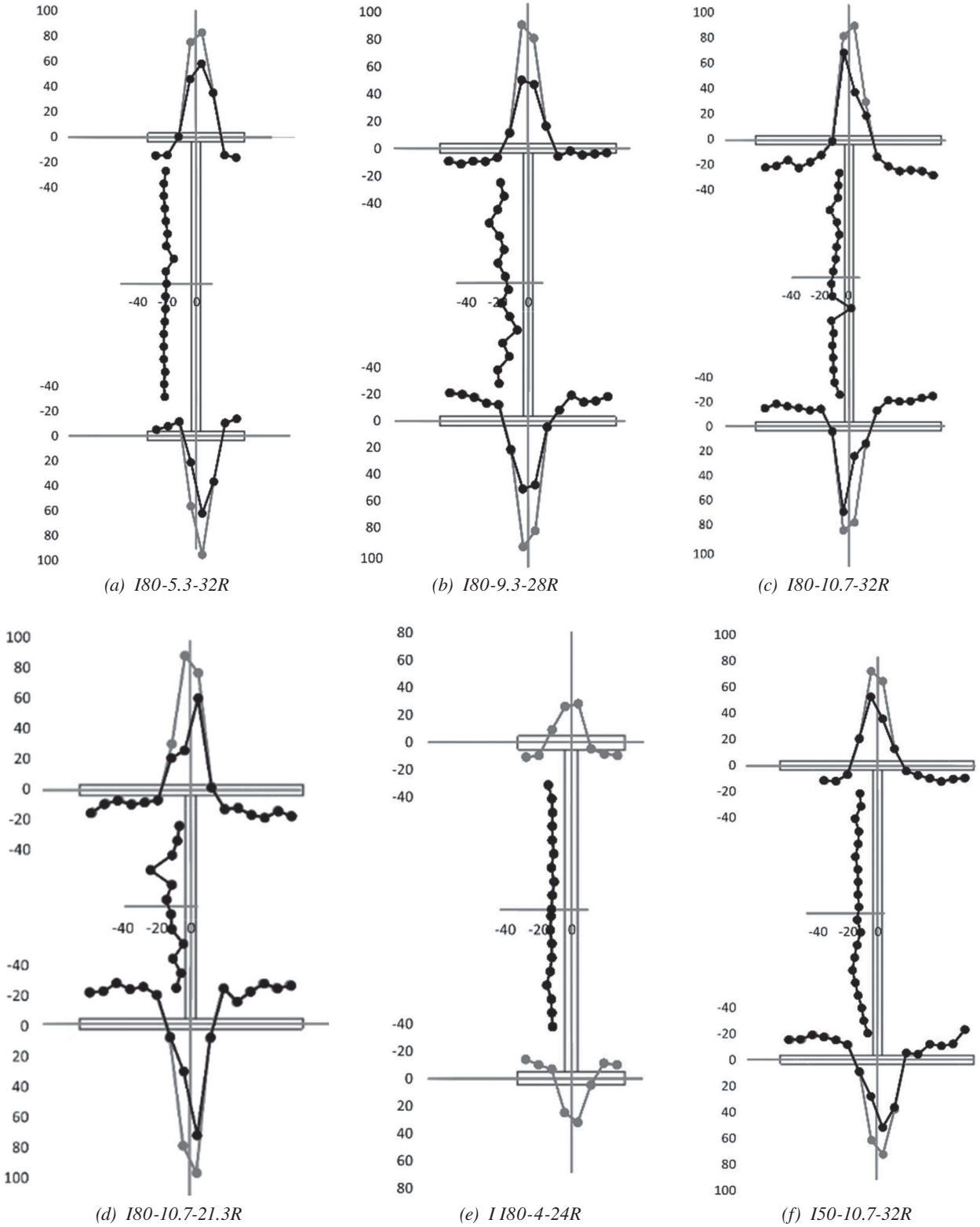

(a) I80-5.3-32R *(b) I80-9.3-28R* *(c) I80-10.7-32R*

(d) I80-10.7-21.3R *(e) I I80-4-24R* *(f) I50-10.7-32R*

Fig. 12. Residual stress measurements (all stress values are ksi).

match these presented results and are excluded for brevity. All other residual stress results not presented in this paper can be found in Clark (2022).

Figure 14 depicts the results and predictive model comparison for specimen I80-4-24R. This specimen is the only one that was fabricated with 0.5 in. thick flanges and web, and its results differ from the trends observed in the other specimens. Figures 14(a) and (b) show the results for the top (*F1*) and bottom (*F2*) flanges, respectively. The compressive stresses in the flanges are much lower than all three of the predictive models. The peak tensile stresses are significantly different from the models as well, with very little tensile stress recorded.

The web compressive stresses are shown in Figure 14(c). The compressive stresses in the web were uniform and were measured to be approximately 12 ksi, which is lower than all three of the predictive models. The closest match for the stresses in the web is the ECCS (1984) model; however, the measured values are about 50% lower than what this model predicts. These differences between the recorded values and predictive models for this specimen may be attributed to the very compact flange ($b/t = 4.0$). Differences may also be attributed to the production process for this plate, as the 0.5 in. plate was produced by a different manufacturer than the 0.375 in. plate. More testing is needed to understand this specimen's anomaly in results relative to the other test results.

Figure 15 shows the comparison of residual stresses between the I80-10.7-32R and I50-10.7-32R specimens. These two specimens are of equal dimensions and section properties, and the only difference between the two is the steel grade. Comparing these two specimens allows for a comparison between the 50 ksi and 80 ksi materials and their influence on residual stresses.

Figures 15(a) and (b) present the residual stresses in the top (*F1*) and bottom (*F2*) flanges, respectively. The maximum tensile stress in the flange for the 80 ksi section is approximately 70 ksi, or $0.875F_y$, while the maximum tensile stress in the 50 ksi section is 54 ksi, which is approximately equal to F_y. The average compressive stresses in the flanges are 20 ksi and 12 ksi for the 80 ksi and 50 ksi sections, respectively. These stresses equate to $0.25F_y$ for both materials. Figure 15(c) depicts the residual stresses in the web for the two sections. The average web compressive stress in the 80 ksi section is approximately 10 ksi ($0.125F_y$), and the average in the 50 ksi section is 13 ksi ($0.26F_y$).

A comparison of the residual stress values in each section shows that the flange compressive stresses increased proportionally to the increase in yield strength of the material. However, the maximum tensile stress in the flange and compressive stress in the web did not increase proportional to the increase in yield strength for the 80 ksi material. This comparison shows that the residual stresses among different material grades are generally not proportional to yield

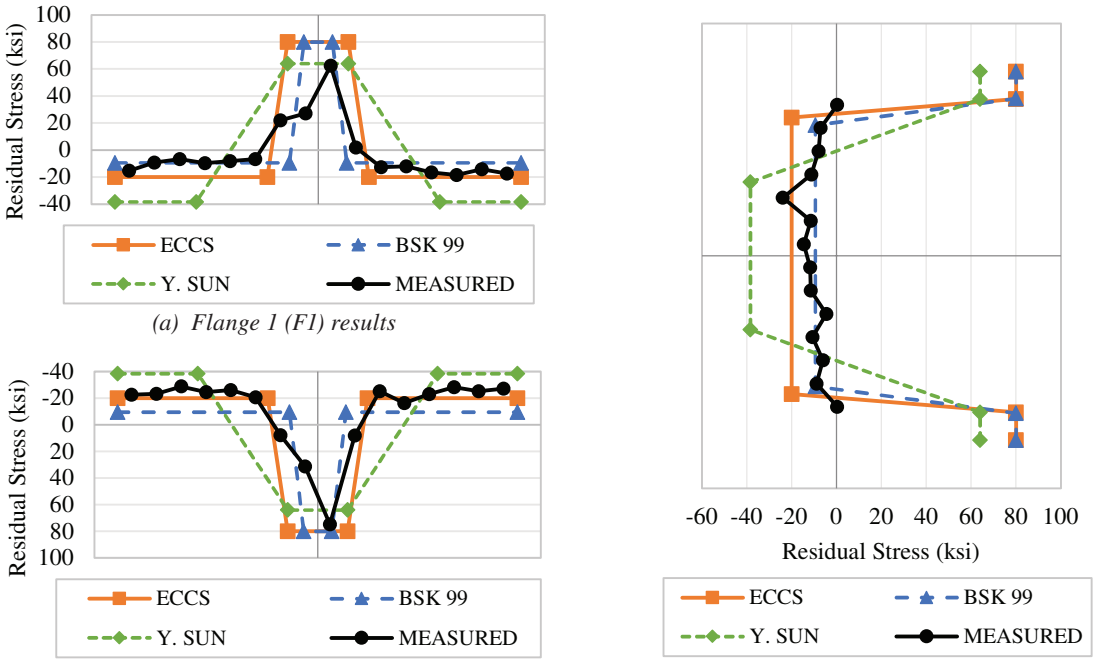

(a) Flange 1 (F1) results

(b) Flange 2 (F2) results

(c) Web results

Fig. 13. Specimen I80-10.7-21.3R residual stress predictive model comparison.

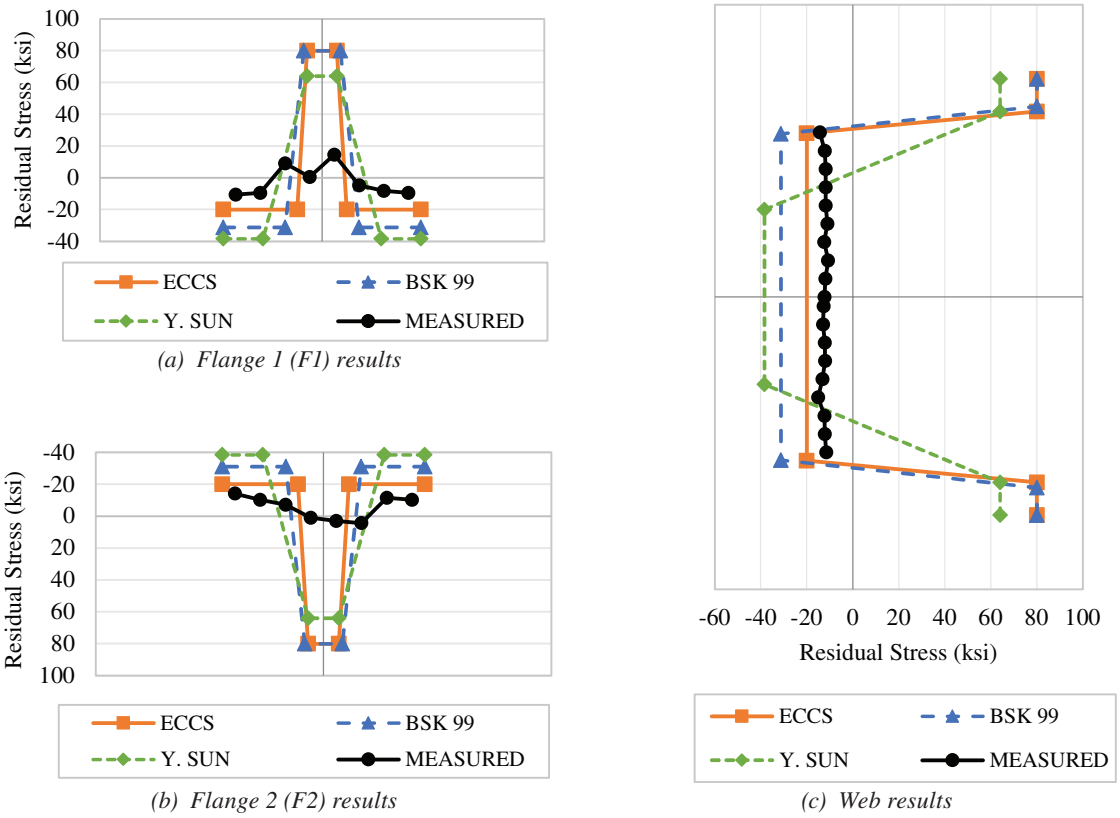

(a) Flange 1 (F1) results

(b) Flange 2 (F2) results

(c) Web results

Fig. 14. Specimen I80-4-24R residual stress predictive model comparison.

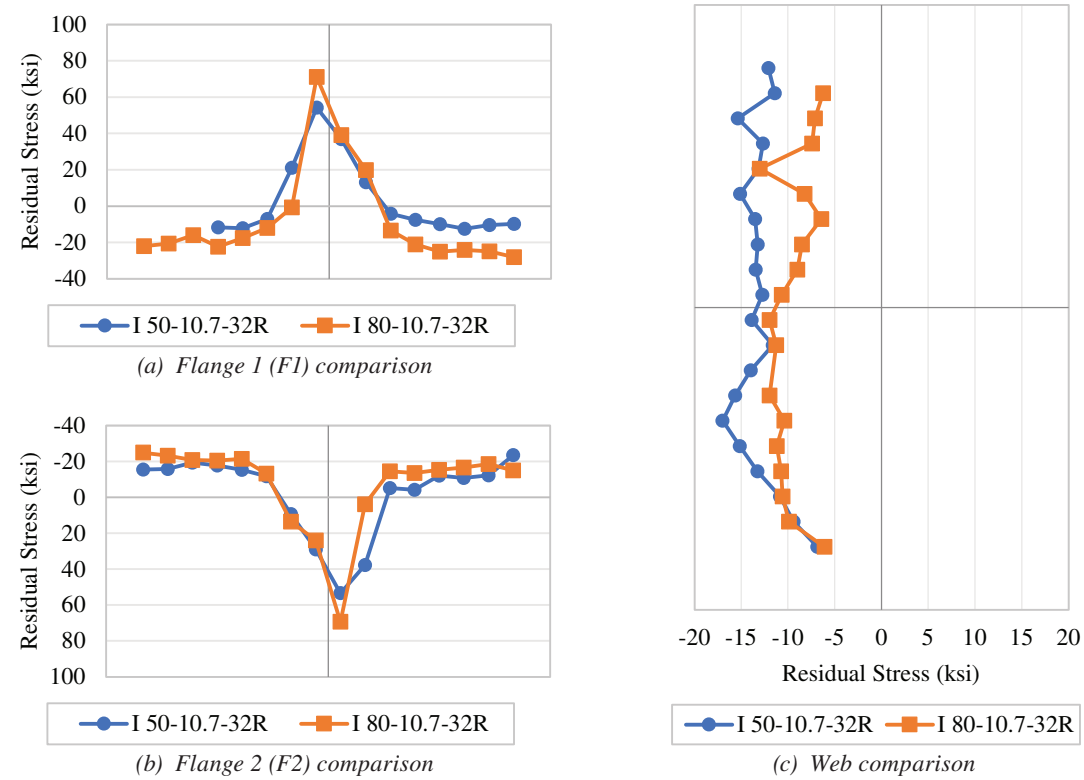

(a) Flange 1 (F1) comparison

(b) Flange 2 (F2) comparison

(c) Web comparison

Fig. 15. Specimen I80-10.7-32R and specimen I50-10.7-32R comparison.

stress, but are more influenced by cross-sectional geometry, as was determined in Schaper et al. (2022).

Results from this study found that the maximum tensile residual stress in the flanges was typically in the 0.75-1.0F_y range, for all specimens except I80-4-24R. The Schaper et al. (2022) study found, however, through a comparison of S460 (65 ksi) and S690 (100 ksi) steel, that the maximum tensile residual stress in the flanges was anywhere from 0.2-0.7F_y. It is worth noting that the specimens studied in the Schaper study were thermal cut, which resulted in tensile residual stresses at the flange tips and could be the cause of the reduced residual stresses at the flange/web interface.

SUMMARY AND CONCLUSIONS

Two different assessments were completed as part of this work using 50 and 80 ksi material—tensile coupon tests and residual stress measurements. Tensile coupon testing was performed on 48 dog bone coupons, and average stress-strain curves were generated for each of the plate materials and thicknesses. All coupons that were tested had a modulus of elasticity of approximately 29,000 ksi. The A572-50 material performed as expected with the curves for each plate thickness being almost identical, while the A656-80 material showed some unanticipated variation between the two thicknesses that can likely be attributed to their different material compositions and manufacturing process. The stress-strain curve for the A656-80 0.5 in. plate material showed almost no yield plateau and had a yield stress that was significantly lower than the A656-80 0.375 in. plate.

Six built-up I-sections underwent residual stress testing, and the results of these tests were compared to three previously published residual stress predictive models. Results showed that the ECCS model was the best predictor of residual stresses in the flanges of sections with larger b/t ratios (b/t = 10.7). The ECCS model also proved to be the best comparison for the 50 ksi material as well. For sections with slightly smaller b/t ratios (b/t = 9.3), the BSK99 model was the best predictor, while none of the models showed to be good predictors of sections with the smallest b/t ratios (b/t = 5, 4.3). A comparison of the Gr. 50 and Gr. 80 sections showed that residual stresses of built-up I-shapes are controlled more by cross-sectional geometry than by the nominal stress of the material.

Future Work

The specimens outlined in this work will be subjected to stub column testing in order to evaluate the cross-sectional slenderness limits and local buckling behavior of high-strength steel sections under compressive load. Additional residual stress studies using the 0.5 in. plate is warranted to understand the anomaly in results relative to the other test results. Further experimental testing and detailed analytical studies are needed for other material grades and larger cross sections to fully understand its behavior as compression members in buildings.

ACKNOWLEDGMENTS

This work was performed at the University of Cincinnati Large-Scale Test Facility and the Ground Floor Makerspace. The authors would like to acknowledge the support of the American Institute of Steel Construction (AISC) for providing the steel plate material. The support of the Lincoln Electric Company (Cleveland, Ohio) is also recognized for providing the fabrication and welding of the built-up sections.

REFERENCES

AISC (2019), "Task Group Report on: High Strength Steel," prepared by the AISC Committee on Specifications Ad Hoc Task Group on High Strength Steel, December 19, American Institute of Steel Construction, Chicago, Ill.

AISC (2022), *Specification for Structural Steel Buildings*, ANSI/AISC 360-22, American Institute of Steel Construction, Chicago, Ill.

ArcelorMittal (2019), "High-Rise Building Brochure," ArcelorMittal Europe—Long Products, Sections and Merchant Bars, Luxembourg.

ASTM (2019), *Standard Specification for High-Strength Low-Alloy Steel Shapes of Structural Quality, Produced by Quenching and Self-Tempering Process (QST)*, ASTM A913/A913M, ASTM International, West Conshohocken, Pa.

ASTM (2020), *Standard Test Methods and Definitions for Mechanical Testing of Steel Products*, ASTM A370, ASTM International, West Conshohocken, Pa.

ASTM (2021), *Standard Specification for High-Strength Low-Alloy Columbium-Vanadium Structural Steel*, ASTM A572/A572M, ASTM International, West Conshohocken, Pa.

ASTM (2022), *Standard Specification for Structural Steel Shapes*, ASTM A992/A992M, ASTM International, West Conshohocken, Pa.

ASTM (2024), *Standard Specification for Hot-Rolled Structural Steel, High-Strength Low-Alloy Plate with Improved Formability*, ASTM A656/A656M, ASTM International, West Conshohocken, Pa.

Ban, H., Shi, G., Bai, Y., and Wang, Y. (2013), "Residual Stress of 460 MPa High Strength Steel Welded I Section: Experimental Investigation and Modeling," *International Journal of Steel Structures*, Vol. 13, No. 4, pp. 691–705.

Ban, H., Shi, G., Shi, Y., and Wang, Y. (2011), "Research Progress on the Mechanical Property of High Strength Structural Steels," *Advanced Materials Research*, Vol. 250–253, pp. 640–648. doi:10.4028/www.scientific.net/AMR.250-253.640

Beg, D. and Hladnik, L. (1996), "Slenderness Limit of Class 3 I Cross-Sections Made of High Strength Steel," *Journal of Constructional Steel Research*, Vol. 38, No. 3, pp. 201–217.

Boverket (2003), *Swedish Regulations for Steel Structures*, BSK 99, Boverket, Karlskrona, Sweden.

Clark, A. (2022), "Material Characterization of High Strength Structural Steel for Building Applications," MS Thesis, University of Cincinnati, Cincinnati, Ohio.

ECCS (1984), "Ultimate Limit State Calculation of Sway Frames with Rigid Joints," Technical Committee 8, Publication No. 33, European Convention for Constructional Steelwork, Brussels, Belgium.

Liu, X. (2017), "Structural Effects of Welding onto High Strength S690 Steel Plates and Welded Sections," PhD Thesis, Hong Kong Polytechnic University, Hong Kong.

NSC (2015), "High Strength Steel," Technical Paper, New Steel Construction, London, United Kingdom.

Rasmussen, K.J.R. and Hancock, G.J. (1995), "Tests of High Strength Steel Columns," *Journal of Constructional Steel Research*, Vol. 34, No. 1, pp. 27–52.

Sampath, K. (2006), "An Understanding of HSLA-65 Plate Steels," *Journal of Materials Engineering and Performance,* ASM International, Vol. 51, No. 1, pp. 32–40.

Schaper, L., Tankova, T., Simoes da Silva, L., and Knobloch, M. (2022), "A Novel Residual Stress Model for Welded I-Sections," *Journal of Constructional Steel Research*, Vol. 188.

Simoes da Silva, L., Tankova, T., and Rodrigues, F. (2021), "Research Report on the Results from the Experimental Programme on Members in HSS," STROnger Steels in the Built Environment (STROBE) Deliverable D3.1.

Sun, Y., Liang, Y., and Zhao, O. (2019), "Testing, Numerical Modelling and Design of S690 High Strength Steel Welded I-Section Stub Columns," *Journal of Constructional Steel Research*, Vol. 159, pp. 521–533.

Wang, K. (2018), "Study on Structural Behaviour of High Strength Steel S690 Welded H- and I-Sections," PhD Thesis, Hong Kong Polytechnic University, Hong Kong.

Wang, Y., Li, G., Chen, S., and Sun, F. (2012), "Experimental and Numerical Study on the Behavior of Axially Compressed High Strength Steel Columns with H-Section," *Engineering Structures*, Vol. 43, pp. 149–159.

Ziemian, R. (2010), *Guide to Stability Design Criteria for Metal Structures*, 6th Ed., Wiley, New York, N.Y.